Journal of Quality Measurement and Analysis *JQMA* 22(SI) 2026, 323-349
e-ISSN: 2600-8602 *http://www.ukm.my/jqma*
https://doi.org/10.17576/jqma.22si.2026.18

MHD CARREAU HYBRID NANOFLUID THIN FILM FLOW OVER AN UNSTEADY ACCELERATED SURFACE WITH A GENERAL SURFACE TEMPERATURE

(*Aliran Filem Nipis Nanobendalir Hibrid Carreau MHD ke Atas Permukaan Dipercepat Tak Mantap dengan Suhu Permukaan Umum*)

DIAN ADLINE JALALUDDIN*, ROSLINDA NAZAR, KOHILAVANI NAGANTHRAN & ISHAK HASHIM

ABSTRACT

In this study, the magnetohydrodynamic (MHD) flow and heat transfer characteristics of a Carreau hybrid nanofluid thin film over an unsteady accelerated stretching surface are numerically investigated using the MATLAB bvp4c solver. The analysis incorporates a general surface temperature varying in both space and time. The hybrid nanofluid consists of titanium dioxide (TiO_2) and copper (Cu) nanoparticles suspended in a carboxymethyl cellulose (CMC)/water-base fluid. The CMC/water-base fluid is assumed to be uniform and initially quiescent, with the flow generated solely by the unsteady stretching of the surface. The results reveal that increasing the Hartmann number (M) reduces fluid velocity, film thickness, and skin friction coefficient due to the opposing Lorentz force, whereas negative magnetic field values enhance flow acceleration and convective heat transfer. Compared to the TiO_2–water nanofluid, the hybrid nanofluid consistently exhibits higher dimensionless temperature profiles and larger local Nusselt numbers, signifying improved surface heat transfer performance. Furthermore, increasing the power-law index (n) and unsteadiness parameter (ω) leads to thicker thermal boundary layers and elevated temperature retention within the thin film, while simultaneously modifying the surface heat transfer rate. Overall, the inclusion of hybrid nanoparticles significantly improves thermal and momentum transport characteristics, demonstrating their effectiveness for controlling heat transfer and flow behavior in unsteady MHD thin film applications.

Keywords: thin film; hybrid nanofluid; magnetohydrodynamic (MHD); Carreau fluid; general surface temperature

ABSTRAK

Dalam kajian ini, ciri-ciri aliran magnetohidrodinamik (MHD) dan pemindahan haba bagi filem nipis nanobendalir hibrid Carreau ke atas permukaan regangan dipercepat tak mantap dikaji secara berangka menggunakan penyelesai bvp4c dalam MATLAB. Analisis ini mengambil kira suhu permukaan umum yang berubah mengikut ruang dan masa. Nanobendalir hibrid tersebut terdiri daripada zarah nano titanium dioksida (TiO_2) dan kuprum (Cu) yang terampai dalam bendalir asas karboksimetil selulosa (CMC)/air. Bendalir asas CMC/air diandaikan seragam dan pada keadaan awal pegun, dengan aliran dijana sepenuhnya oleh regangan tak mantap permukaan. Keputusan menunjukkan bahawa peningkatan nombor Hartmann (M) mengurangkan halaju bendalir, ketebalan filem, dan pekali geseran permukaan akibat tindakan daya Lorentz yang menentang aliran, manakala nilai medan magnet negatif meningkatkan pecutan aliran dan pemindahan haba secara perolakan. Berbanding nanobendalir TiO_2–air, nanobendalir hibrid secara konsisten menunjukkan profil suhu tak berdimensi yang lebih tinggi serta nombor Nusselt setempat yang lebih besar, yang menandakan prestasi pemindahan haba permukaan yang lebih baik. Selain itu, peningkatan indeks kuasa (n) dan parameter ketakmantapan (ω) menyebabkan lapisan sempadan terma menjadi lebih tebal dan meningkatkan pengekalan suhu dalam filem nipis, di samping mempengaruhi kadar pemindahan haba pada permukaan. Secara keseluruhannya, kehadiran nanopartikel hibrid meningkatkan dengan ketara ciri pemindahan haba dan momentum, sekali gus menunjukkan keberkesanannya dalam mengawal pemindahan haba dan tingkah laku aliran dalam aplikasi filem nipis MHD tak mantap.

Kata kunci: filem nipis; nanobendalir hibrid; magnetohidrodinamik (MHD); bendalir Carreau; suhu permukaan umum

1. Introduction

Thin film flow is used in various fields due to its ability to create a thin, continuous layer of liquid over surfaces. Its significance lies in enhancing heat and mass transfer efficiency, particularly in systems where controlled thermal behavior is critical. In chemical engineering, it aids in efficient heat transfer, making it ideal for reactors, evaporators, and dryers, particularly for heat-sensitive substances. It is also key in electronics, with applications in microelectronics, displays, and thin film batteries. Optical coatings benefit from thin film technology for antireflective layers on lenses and solar panels. In medicine, it helps in drug delivery systems and coatings for implants, while mechanical uses include lubrication and heat exchangers. Additionally, thin films play a role in water desalination and fuel cells, showing their versatility across different industries. Understanding the dynamics of thin film flow is therefore essential for optimizing system performance, improving energy efficiency, and ensuring process stability. Wang (1990) was the first to explore the hydrodynamic behavior of flow within a thin liquid film induced by an unsteady stretching surface. Andersson *et al*. (2000) later expanded on this groundbreaking research by incorporating the analysis of heat transfer in a thin liquid film. This line of study was further developed by Liu & Andersson (2008), who examined a more general case involving variations in prescribed temperature. Extensive research on thin film has been conducted by Jalaluddin *et al*. (2023), Ullah *et al*. (2023), Jazaa *et al*. (2024), and Alharbi *et al*. (2024), as documented in their various studies. Janthe *et al*. (2024) recently explored how thermocapillary effects, magnetic fields, and heat dynamics influence thin film flow on a moving surface. This study shows that magnetic fields slow thin film flow, while thermocapillary effects reduce horizontal movement near the surface. Thermal radiation can reverse flow, and higher Joule dissipation lowers fluid temperature, offering insights for improving thin film coating processes.

In parallel, hybrid nanofluids have emerged as advanced working fluids with enhanced thermophysical and rheological properties, offering superior heat transfer performance compared to conventional fluids. A base fluid and two or more kinds of nanoparticles are mixed to create hybrid nanofluids, which are sophisticated fluids with improved thermal characteristics. This research area has gained traction due to its potential applications in various industries, including heat exchangers, energy storage, and cooling systems. To increase heat transfer, an innovative concept of a metal component suspended in liquid at the nanoscale was introduced by Choi & Eastman (1995). The studies were conducted by Suresh *et al*. (2011), and Sundar *et al*. (2014) proposed a hybrid nanofluid as a solution to this problem. In heat transfer applications, hybrid nanofluids, particularly those combining copper (Cu) and titanium dioxide (TiO_2), have gained significant attention in thermal management due to their superior thermal properties in contrast to conventional fluids. The addition of multiple nanoparticles boosts thermal conductivity and heat transfer, improving performance in engineering applications like cooling systems and heat exchangers. Cu's high thermal conductivity, combined with TiO_2's stability, significantly boosts the thermal performance of these fluids. With multi-walled carbon nanotubes (MWCNT) and silica nanoparticles, Che Sidik *et al*. (2020) observed rises in thermal conductivity of up to 23.3% and 8.8%, respectively, indicating that Cu-TiO_2 has a similar potential. Waini *et al*. (2021) highlighted their success in cooling electronics, where they outperform single-component nanofluids. Factors like nanoparticle shape, size, concentration, and the application of magnetohydrodynamic (MHD) principles in hybrid nanofluids have captured the interest of many scientists because of their improved heat transfer capabilities, promising thermal properties, and wide-ranging potential applications (Takabi & Salehi 2014; Zainal *et al*. 2020a; Zainal *et al*. 2020b; Bing Kho *et al*. 2023; Islam *et al*. 2023). Recently, Sheik *et al*. (2026) further confirm that hybrid nanofluids can enhance heat transfer performance by up to 60%, although challenges such as nanoparticle stability and agglomeration remain significant.

The Carreau model, introduced by Carreau (1972), describes the behavior of non-Newtonian fluids with shear-dependent viscosity. This model is particularly suitable for capturing complex rheological behavior in thin film flows, where viscosity varies with shear rate. Several researchers have explored the applications of the Carreau liquid model to several scientific advancements and natural phenomena. Myers (2005) found that this model is highly accurate for describing thin film flow, making it the preferred choice for generalized non-Newtonian fluids. Consequently, numerous significant studies have been published on the flow of Carreau thin films (Sulochana & Ashwinkumar 2017; Iqbal *et al*. 2020; Bilal *et al*. 2021). Research has extensively focused on the thermophysical properties of Carreau fluids in thin film scenarios, particularly under the influence of external factors like thermal gradients and magnetic fields. For example, Naganthran *et al*. (2021) investigated the thermocapillary effects in a Carreau thin hybrid nanofluid film flow, highlighting the impact of thermal gradients on flow dynamics and heat transfer properties. Similarly, Gul *et al*. (2021) examined the magnetohydrodynamic (MHD) effects on Carreau thin film flow, demonstrating how magnetic fields can alter the flow behavior and enhance heat transfer. The interaction between thermocapillarity and MHD remains a prominent theme in the literature, highlighting the complex nature of Carreau fluid dynamics. Furthermore, the mathematical modeling of Carreau fluid flow has been advanced through various analytical and numerical techniques. The bvp4c function in MATLAB has been employed to derive solutions for the flow of Carreau fluids over-stretching surfaces, providing insights into the effects of different boundary conditions and flow configurations (Naganthran *et al*. 2020a; Naganthran *et al*. 2020b). These models are crucial for predicting the behavior of Carreau fluids in practical applications, as they account for the complex interactions between fluid properties and external forces.

Magnetohydrodynamic (MHD) flow has attracted considerable attention due to its wide range of applications in engineering systems such as metallurgy, energy systems, and cooling technologies. The interaction between magnetic fields and electrically conducting fluids generates a Lorentz force that significantly influences flow behavior and heat transfer. This interaction provides a controllable mechanism for regulating fluid motion and thermal performance in thin film systems. This interaction provides a controllable mechanism for regulating fluid motion and thermal performance in thin film systems. Numerous studies have explored MHD effects in nanofluids (Tayebi *et al*. 2021; Abderrahmane *et al*. 2022; Chabani *et al*. 2022; Alabdulhadi *et al*. 2023; Thirumalaisamy & Reddy 2023). Thus, the interaction between magnetic fields and fluid dynamics is another critical aspect of MHD thin film flow. Studies have demonstrated that applying a magnetic field can enhance or suppress flow velocities, depending on the fluid's properties and the magnetic field strength. For instance, Ullah *et al*. (2018) explored the nanofluids flow in the presence of a magnetic field and found that the magnetic field's strength is a key factor in determining the flow characteristics and heat transfer efficiency. Similarly, Kamis *et al*. (2022) analyzed the hybrid nanofluid boundary layer flow in a thin film over an unsteady stretched permeable sheet, applying computational methods to derive the governing equations. This aligns with the findings of Naganthran *et al*. (2023), who investigated thermocapillarity in Cross hybrid nanofilm flow, indicating that the thermal characteristics of the fluid can be significantly impacted by the presence of nanoparticles. Recent studies have further highlighted the significant role of magnetohydrodynamic effects in hybrid nanofluid systems. More recent studies by Zainal *et al*. (2021), Zainal *et al*. (2025), and Shahzad & Alosaimi (2026) further confirm that MHD effects, suction, and geometric parameters can significantly influence dual solutions, skin friction, and heat transfer performance in hybrid nanofluid flows.

Despite these advancements, studies incorporating general surface temperature variations remain relatively limited. Wang (2006) provided early analytical solutions using the homotopy analysis method, while Liu & Andersson (2008) emphasized the role of thermocapillarity under varying temperature conditions. Noor *et al*. (2010) and Aziz & Hashim (2010) further extended these analyses by incorporating magnetic effects and viscous dissipation. Aziz *et al*. (2018) and Chandra Roy (2020) demonstrated that surface temperature variations significantly influence heat transfer and flow behavior. These findings highlight the importance of incorporating realistic temperature boundary conditions in thin film modeling. Further studies, such as those by Vemula *et al*. (2016), have examined the implications of variable surface temperatures on nanofluid flow, noting that different fluids, including water and organic solvents, exhibit varying heat transfer characteristics. Sadiq (2021) also contributed to this discourse by analyzing heat transfer in nanoliquid thin films with internal heat generation, reinforcing the importance of surface temperature in dictating thermal behavior.

However, most existing studies have examined Carreau fluids, hybrid nanofluids (Cu-TiO_2-water), MHD effects, and general surface temperature independently or in limited combinations. The simultaneous interaction of these effects in an unsteady thin film configuration remains insufficiently explored. This gap limits the applicability of current models to real-world systems, where such effects occur concurrently. Therefore, the present study aims to address this gap by developing a comprehensive mathematical model for unsteady MHD Carreau hybrid nanofluid thin film flow over a stretching surface with a general surface temperature. The novelty of this work lies in the simultaneous consideration of Carreau non-Newtonian behavior, hybrid nanoparticle interaction, magnetic field effects, and spatial–temporal temperature variation within a unified framework. In summary, this study investigates the influence of key governing parameters, including the Hartmann number, power-law index, unsteadiness parameter, and temperature indices, on velocity, temperature distribution, film thickness, skin friction, and heat transfer rate. A comparative analysis between hybrid nanofluid and conventional nanofluid is also conducted to evaluate thermal performance enhancement and to highlight the role of hybrid nanoparticles in advanced thin film applications.

2. Problem formulation

In this study, the two-dimensional Carreau hybrid nanofilm flow initiates from a narrow opening at the Cartesian coordinate system's origin, considering the effects of magnetohydrodynamics (MHD) and a general surface temperature, as depicted in Figure 1. There is a thin liquid film and a horizontally oriented accelerating sheet that contain this flow. The thin liquid film is assumed to have a time-dependent thickness, denoted by $h(t)$, while the flow is considered unsteady and incompressible. The Cartesian coordinates consist of the $x-$axis and $y-$axis, where the $y-$axis is perpendicular to the plate, and the $x-$axis is aligned with it. The plate is positioned at $y=0$. The thin film is both accelerated and stretched, as described by the velocity equation

$$U_w\left(x,t\right)=\frac{bx}{\left(1-kt\right)}, \tag{1}$$

where b and k are positive constants with dimensions time^{-1}, $kt \neq 1$. Here, $b>0$ indicates the initial stretching rate of the surface, while k characterizes the unsteadiness (acceleration) of the stretching process. Consequently, k^{-1} becomes the representative time scale of the resulting unsteady boundary-layer problem. The adopted formulation of the sheet velocity $U_w\left(x,t\right)$ in Eq. (1) s physically meaningful only for the finite time interval $0 \leq t < 1/k$, or which the surface velocity remains bounded (unless $k=0$, which reduces the problem to the steady stretching case). The thermal properties of the elastic sheet are allowed to vary both along the sheet and with time, as governed by the temperature equation. The temperature of the stretching surface, T_s, is presumed to differ as a function of the streamwise coordinate x, measured from the slit at the origin, as well as time,

$$T_s=T_0-T_{ref}\frac{bx^r}{\nu_f}\left(1-kt\right)^{-m}, \tag{2}$$

where T_{ref} is a constant reference temperature, taken as $T_{ref}=T_0$ in the present analysis, and T_0 refer the temperature at the slit located at $x=0$ (except for the special case $r=0$). The parameter b is a positive constant of proportionality with the dimension (length^{2-r} time^{-1}), and r and m are positive power indices that characterize the spatial and temporal variations of the surface temperature, respectively. Here, ν_f denotes the kinematic viscosity of the base fluid (CMC/water). Additionally, the effects of gravity are assumed to be minimal and are therefore not included. The boundary layer model developed in this research remains valid only if the thickness of the liquid film and the boundary layer do not overlap; if not, the model appears inconsistent (Maity *et al.* 2016) . Furthermore, it is assumed that the thin liquid layer is wave-free and smooth (Andersson *et al.* 2000). These assumptions are commonly adopted in thin film flow analyses, where the film thickness is sufficiently small and the flow is predominantly driven by surface stretching and magnetohydrodynamic forces, rendering gravitational and surface wave effects negligible in comparison.

It is also assumed that the magnetic Reynolds number is low enough to disregard the magnetic field induced, and the absence of an electric field is taken into consideration. For the hybrid nanofluid, which consists of a stable mixture of nanoparticles and the base fluid, it is presumed that the nano-particles are of uniform size, and the impact of agglomeration of nanoparticles on thermophysical characteristics is ignored. This assumption is reasonable for low nanoparticle volume fractions and well-dispersed suspensions, where agglomeration and sedimentation effects are minimal and have a negligible influence on the overall thermophysical behavior of the nanofluid. Moreover, the thermophysical properties of the hybrid nanofluid are assumed to be constant, which is appropriate for moderate temperature variations typically encountered in thin film heat transfer applications. While these assumptions may limit the applicability of the model under extreme operating conditions, they enable clear physical interpretation of the dominant mechanisms governing unsteady MHD Carreau hybrid nanofluid thin film flow.

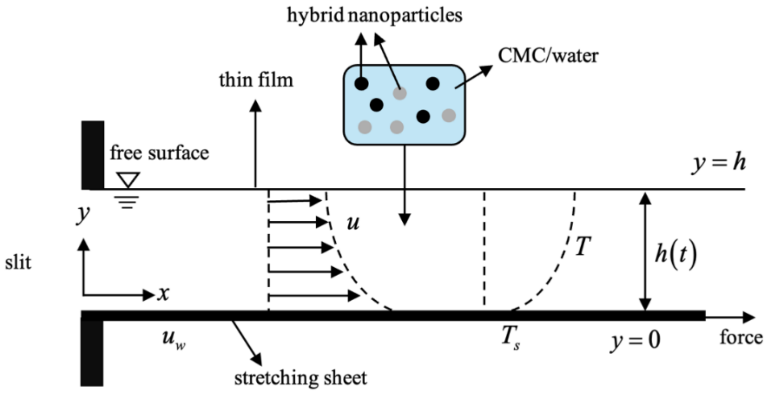

Figure 1: A physical diagram of thin film

A Carreau fluid moving over a stretched hot plate is mathematically modeled; the Cauchy stress tensor for this type of fluid is denoted as (Myers 2005)

$$\tau = -p\mathbf{I} + \eta\mathbf{A_1}, \tag{3}$$

where

$$\eta = \eta_\infty + (\eta_0 - \eta_\infty)\left[1 + (\lambda\dot{\gamma})^2\right]^{\frac{n-1}{2}}. \tag{4}$$

In this context, $\mathbf{I}$ represent the identity tensor and p denote the pressure. The parameters η_∞ and η_0 correspond to the infinite-shear-rate viscosity and zero-shear-rate viscosity, respectively, while n is the power-law index and λ represents the material time constant. The shear rate, $\dot{\gamma}$ is denoted by

$$\dot{\gamma} = \sqrt{\frac{1}{2}(\dot{\gamma} : \dot{\gamma})} = \sqrt{\frac{1}{2}\Pi} = \sqrt{\frac{1}{2}tr\left(\mathbf{A}_1^2\right)} = \sqrt{\frac{1}{2}\sum_i \sum_j \dot{\gamma}_{ij}\dot{\gamma}_{ji}}. \tag{5}$$

Here, Π represents the tensor of the second invariant strain rate, and $\mathbf{A_1}$ is the Rivlin–Ericksen tensor, which is further expressed as

$$\mathbf{A_1} = (\text{grad}\,\mathbf{V}) + (\text{grad}\,\mathbf{V})^{\mathrm{T}}. \tag{6}$$

We focus on situations where $\eta_0 \gg \eta_\infty$, which occur most frequently. Typically, the value of η_∞ is deemed through extrapolation or set to zero, as recommended theoretically (Boger 1977). Consequently, in this study, η_∞ is set to zero, which simplifies Eq. (3), transforming the expression for the Cauchy stress tensor become

$$\tau = -p\mathbf{I} + \eta_0\left[1 + (\lambda\dot{\gamma})^2\right]^{\frac{n-1}{2}}\mathbf{A_1}. \tag{7}$$

The Carreau fluid model exhibits pseudoplastic, dilatant, and Newtonian behaviors for $0<n<1,\ n>1$, and $n=1$, respectively, where n is the power-law index. In the unsteady case, denoted as $B(t)=B_0(1-kt)^{-1/2}$, a magnetic field is considered in the transverse direction. The governing equation for the Carreau fluid's liquid film flow is described as below.

Continuity equation is

$$\frac{\partial u}{\partial x}+\frac{\partial v}{\partial y}=0. \tag{8}$$

Momentum equation is

$$\begin{aligned}\frac{\partial u}{\partial t}+u\frac{\partial u}{\partial x}+v\frac{\partial u}{\partial y}&=\frac{\mu_{hnf}}{\rho_{hnf}}\frac{\partial^2 u}{\partial y^2}\left[1+\lambda^2\left(\frac{\partial u}{\partial y}\right)^2\right]^{\frac{n-1}{2}}\\&+\frac{\mu_{hnf}}{\rho_{hnf}}(n-1)\lambda^2\frac{\partial^2 u}{\partial y^2}\left(\frac{\partial u}{\partial y}\right)^2\left[1+\lambda^2\left(\frac{\partial u}{\partial y}\right)^2\right]^{\frac{n-3}{2}}-\frac{\sigma_{hnf}}{\rho_{hnf}}B^2u.\end{aligned} \tag{9}$$

Energy equation is

$$\frac{\partial T}{\partial t}+u\frac{\partial T}{\partial x}+v\frac{\partial T}{\partial y}=\frac{k_{hnf}}{(\rho C_p)_{hnf}}\frac{\partial^2 T}{\partial y^2}, \tag{10}$$

subject to the following initial and boundary conditions:

$$\begin{aligned}&u=U_w(x,t),\quad v=0,\quad T=T_s\quad \text{at}\quad y=0,\\&\mu_{hnf}\frac{\partial u}{\partial y}=0,\quad \frac{\partial T}{\partial y}=0,\quad v=\frac{dh}{dt}\quad \text{at}\quad y=h,\end{aligned} \tag{11}$$

where u and v represent the velocity components of the hybrid nanofluid along the $x-$ and $y-$ directions, respectively. The parameter n denotes the power-law index, T is the temperature of the hybrid nanofluid, and λ is the material time constant. Additionally, k_{hnf}, ρ_{hnf}, μ_{hnf}, σ_{hnf} and $(\rho C_p)_{hnf}$ denote the thermal conductivity, density, dynamic viscosity, electrical conductivity, and heat capacity of the hybrid nanofluid, respectively. The further definitions and numerical values of these thermophysical properties are provided in Table 1 and Table 2. At $y=h$, a kinematic constraint is imposed on the fluid motion, expressed as $v=dh/dt$. At the adiabatic free surface, both the wall shear stress and heat flux vanish, leading to the boundary conditions $\partial T/\partial y=\partial u/\partial y=0$ at $y=h$. These boundary conditions ensure physically consistent momentum and thermal behavior at the free surface.

Table 1 summarizes the thermophysical properties of the base fluid and nanoparticles adopted from the literature. Table 2 presents the effective thermophysical properties of the nanofluid and hybrid nanofluid employed in the present study, based on a TiO_2-Cu/CMC–water formulation. Meanwhile, the physical properties of the copper (Cu) and titanium dioxide (TiO_2) hybrid nanofluids, as well as the base fluid, sodium carboxymethyl cellulose (CMC/water) are also listed therein. The model can be reduced to a regular (Newtonian) fluid by setting the nanoparticle volume fraction $\phi = 0$. The equation $\phi_{hnf} = \phi_1 + \phi_2$ represents the hybrid nanofluid's overall volume concentration of the two kinds of nanoparticles, where ϕ_1 and ϕ_2 represent the volume fractions of TiO_2 and Cu nanoparticles, respectively. Furthermore, k_f and k_{hnf} denote the thermal conductivities of the base fluid and hybrid nanofluid, respectively, while ρ_f and ρ_{hnf} correspond to their densities. Similarly, $\left(\rho C_p\right)_f$ and $\left(\rho C_p\right)_{hnf}$ represent the heat capacities of the base fluid and the hybrid nanofluid. Based on physical considerations, these correlations align with the concepts of mass and energy conservation.

Table 1: The correlation properties of the hybrid nanofluid (Takabi & Salehi 2014)

Properties	TiO_2-Cu/(CMC/H_2O) mathematical relation
Density	$\rho_{hnf} = \left(1-\phi_{hnf}\right)\rho_f + \phi_1\rho_{s1} + \phi_2\rho_{s2}$
Dynamic viscosity (Brinkman model)	$\mu_{hnf} = \dfrac{\mu_f}{\left(1-\phi_{hnf}\right)^{2.5}}$
Thermal capacity	$\left(\rho C_p\right)_{hnf} = \left(1-\phi_{hnf}\right)\left(\rho C_p\right)_f + \phi_1\left(\rho C_p\right)_{s1} + \phi_2\left(\rho C_p\right)_{s2}$
Thermal conductivity (Maxwell model)	$\dfrac{k_{hnf}}{k_f} = \left[\dfrac{\left(\dfrac{\phi_1 k_{s1} + \phi_2 k_{s2}}{\phi_{hnf}}\right) + 2k_f + 2\left(\phi_1 k_{s1} + \phi_2 k_{s2}\right) - 2\phi_{hnf} k_f}{\left(\dfrac{\phi_1 k_{s1} + \phi_2 k_{s2}}{\phi_{hnf}}\right) + 2k_f - \left(\phi_1 k_{s1} + \phi_2 k_{s2}\right) + \phi_{hnf} k_f}\right]$
Electrical conductivity	$\dfrac{\sigma_{hnf}}{\sigma_f} = \left[\dfrac{\left(\dfrac{\phi_1 \sigma_{s1} + \phi_2 \sigma_{s2}}{\phi_{hnf}}\right) + 2\sigma_f + 2\left(\phi_1 k_{s1} + \phi_2 k_{s2}\right) - 2\phi_{hnf} k_f}{\left(\dfrac{\phi_1 \sigma_{s1} + \phi_2 \sigma_{s2}}{\phi_{hnf}}\right) + 2\sigma_f - \left(\phi_1 \sigma_{s1} + \phi_2 \sigma_{s2}\right) + \phi_{hnf} \sigma_f}\right]$

In Table 2, ρ denotes density, C_p specific heat capacity, k thermal conductivity, σ electrical conductivity, and $\hat{\beta}$ thermal expansion coefficient. Subscripts f , $s1$, and $s2$ refer to the base fluid, first nanoparticle, and second nanoparticle, respectively. Thermophysical properties are adopted from Oztop & Abu-Nada (2008) and Das & Jana (2015).

Table 2: The base fluid (sodium carboxymethyl cellulose (CMC)/water) and selected nanoparticles' thermophysical properties (Oztop & Abu-Nada 2008; Das & Jana 2015)

Properties	$\rho\left(\text{kg/m}^3\right)$	$k\left(\text{W/mK}\right)$	$\hat{\beta}\times10^{-5}\left(\text{mK}\right)$	$\sigma\left(S/m\right)$	$C_p\left(\text{J/kgK}\right)$
TiO_2	4250	8.9538	0.9	2.6×10^{6}	686.2
Cu	8933	400	1.67	5.96×10^{6}	385
CMC/H_2O (0-0.3%)	997.1	0.613	21	5.5×10^{-6}	4179

Next, we present the following similarity transformations (Liu & Andersson 2008)

$$\psi = xf(\eta)\sqrt{\frac{\nu_f b}{1-kt}}, \qquad u = \frac{\partial \psi}{\partial y} = \frac{bx}{1-kt}f'(\eta),$$
$$v = -\frac{\partial \psi}{\partial x} = -\beta\sqrt{\frac{\nu_f b}{1-kt}}f(\eta), \qquad T = T_0 - T_{ref}\left(\frac{bx^r}{\nu_f}\right)(1-kt)^{-m}\theta(\eta), \tag{12}$$

$$\eta = \frac{y}{\beta}\sqrt{\frac{b}{\nu_f(1-kt)}}, \tag{13}$$

where the prime symbol depicts differentiation with respect to η. Using the similarity variables from Eqs. (12) and (13), the boundary conditions in Eq. (11), along with Eqs. (9) and (10), are converted into the following ordinary differential equations (ODEs) take the form.

$$\left(\frac{\mu_{hnf}/\mu_f}{\rho_{hnf}/\rho_f}\right)\left(1+\frac{nWe^2}{R}f''^2\right)\left(1+\frac{We^2}{R}f''^2\right)^{\frac{n-3}{2}}f''' + R\left(ff'' - \frac{\omega\eta}{2}f'' - f'^2 - \omega f' - \frac{\sigma_{hnf}/\sigma_f}{\rho_{hnf}/\rho_f}Mf'\right) = 0, \tag{14}$$

$$\frac{k_{hnf}/k_f}{(\rho C_p)_{hnf}/(\rho C_p)_f}\theta'' + R\Pr\left(f\theta' - rf'\theta - \frac{\eta\omega}{2}\theta' - m\omega\theta\right) = 0, \tag{15}$$

subject to the boundary conditions

$$f(0)=0, \quad f'(0)=1, \quad \theta(0)=1,$$
$$f(1)=\frac{\omega}{2}, \quad f''(1)=0, \quad \theta'(1)=0, \tag{16}$$

where

$$\omega = \frac{k}{b}, \; We = \sqrt{\frac{\lambda^2 b^3 x^2}{\nu_f(1-kt)^3}}, \; \Pr = \frac{(C_p)_f \mu_f}{k_f}, \; R = \beta^2, \, M = \frac{\sigma_f B_0^2}{b\rho_f}, \tag{17}$$

wherein ω, We, $\Pr$, R and M are the dimensionless unsteadiness measure, the Prandtl number, the local Weissenberg number, the dimensionless film thickness, and the Hartmann parameter, respectively. Thus, according to the boundary conditions, see Eq. (17), the solution of Eq. (14) for fixed value of δ would be locally similar. According to the local similarity technique, the dimensionless quantity δ is calculated at any $x-$ station, and the upstream flow history's impact on the similarity variable is ignored unless it is significant (Rahman 2011).

Additionally, the dimensionless film thickness is defined by the unknown constant β. At the free surface, since β also represents the value of the similarity variable (η), the expression in Eq. (11) can take the following form:

$$\beta = h\sqrt{\frac{b}{\nu_f(1-kt)}}, \quad \frac{dh}{dt} = -\frac{\beta k}{2}\sqrt{\frac{\nu_f}{b(1-kt)}}. \tag{18}$$

The unknown constant β must be calculated as part of the boundary-value problem, and $\frac{dh}{dt}$ indicates the rate of change in film thickness. When $n=1$ and $We=0$, the Carreau fluid model in Eqs. (14) and (15) exhibits Newtonian behavior. The local skin friction coefficient and local Nusselt number, denoted as (C_{fx}) and (Nu_x), are key physical quantities in this study can be represented as

$$C_{fx} = \frac{\tau_w}{\rho_f (U_w)^2/2}, \quad Nu_x = \frac{q_w x}{k_f T_{ref}}, \tag{19}$$

here, the heat flux from the surface of the sheet (q_w) and the wall shear stress (τ_w) are described by the following equations (Rehman *et al*. 2019)

$$\tau_w = \left\{ \mu_{hnf}\frac{\partial u}{\partial y}\left[1+\lambda^2\left(\frac{\partial u}{\partial y}\right)^2\right]^{\frac{n-1}{2}} \right\}_{y=0}, \quad q_w = -k_{hnf}\left(\frac{\partial T}{\partial y}\right)\bigg|_{y=0}, \tag{20}$$

By applying Eqs. (12) and (13) and substituting Eq. (19) into Eq. (20), the resulting expression is:

$$\begin{aligned} &C_{fx}\,\mathrm{Re}_x^{1/2} = \frac{\mu_{hnf}}{\mu_f}\frac{2}{\sqrt{R}} f''(0)\left\{1+\frac{We^2}{R}\left[f''(0)\right]^2\right\}^{\frac{n-1}{2}}, \\ &Nu_x\,\mathrm{Re}_x^{-3/2}\,\beta(1-kt)^{m-1}x^{2-r}\frac{k_f}{k_{hnf}} = \theta'(0). \end{aligned} \tag{21}$$

The local Reynolds number is defined as $\mathrm{Re}_x = \frac{xU_w(x,t)}{\nu_f}$.

The present analysis is confined to an unsteady stretching surface ($b > 0$), which corresponds to a physically stable forward-flow configuration. Under such conditions, the boundary layer remains attached to the surface, and the governing equations admit a unique solution. Dual or multiple solutions are typically associated with shrinking surfaces ($b < 0$), flow reversal, or strong suction effects, where competing flow structures may arise. Since these conditions are not considered in the current model, no solution multiplicity is observed. Therefore, the results presented in this study correspond exclusively to the physically realizable stable solution branch. The extension of the present framework to shrinking configurations, where dual solutions may exist, is suggested for future investigation.

3. Results and Discussion

This section outlines the numerical results and explains the physical significance of the trends observed in the physical quantities as the relevant parameter values change. The governing mathematical model, represented by ordinary differential equations (Eqs. (14)–(16)), is implemented using the MATLAB bvp4c function. Developed by Shampine *et al.* (2003), this function is known for its robustness in approximating solutions for mathematical models with unknown parameters. For numerical implementation, the higher-order differential equations are first transformed into a system of first-order ordinary differential equations, which are then solved using the collocation-based bvp4c solver with adaptive mesh refinement. The code requires reasonable initial guesses to solve the model and determine the unknown parameters. While solving the model with the bvp4c function, the relative tolerance is set at 1×10^{-10} to guarantee that numerical answers are accurate, approximately 0.001%. The convergence of the solution is verified through mesh refinement, where further refinement produces negligible changes in key physical quantities such as skin friction and heat transfer rate, thereby confirming numerical stability and reliability. All figures and tables are presented with consistent notation and parameter settings to ensure clarity and facilitate comparison. In addition, by setting the governing parameters related to the hybrid nanofluids, there are a total of six physical parameters influencing this flow model, which are the following:

- ω, the unsteadiness parameter $\left(1.2\le\omega\le0.2\right)$.
- n, the power-law index $\left(0\le n\le2.5\right)$.
- M, the Hartmann parameter $\left(-1\le M\le1\right)$.
- We, the local Weissenberg number is fixed at 0.2. As the temperature field does not influence the hydrodynamic problem, this study specifically concentrates on the thermal energy aspect (Liu & Andersson 2008).
- r and m, the positive power indices are fixed at $r=2$ and $m=1.5$.
- Pr, the Prandtl number is set at 6.2 for all computations in this study, as the base fluid used is CMC/water.

Table 3 compares the numerical results with previous studies, showing a strong agreement up to three decimal places. The maximum deviation observed is below 0.4%, confirming both the correctness of the similarity formulation and the robustness of the numerical scheme. The thermophysical properties of the hybrid nanofluid are incorporated into the governing equations using the correlation models listed in Table 1, which account for the combined effects of multiple nanoparticles on density, viscosity, and thermal conductivity. A fixed value of $\phi_{hnf}=\phi_1+\phi_2=0.02+0.01=0.03$ is used for the hybrid nanoparticle volume fraction**.** Here, $\phi_1=0.02$ corresponds to the volume fraction of titanium dioxide (TiO_2) nanoparticles, while $\phi_2=0.01$ represents the volume fraction of copper (Cu) nanoparticles. In contrast, for the single-type nanofluid conditions, the copper nanoparticle volume fraction ϕ_2, is set to zero, and only the TiO_2 nanoparticle is considered. Table 3 validates the current results by comparing them with analytical solutions reported by Wang (2006) and Aziz & Hashim (2010), demonstrating strong agreement and confirming the accuracy of the numerical approach. Meanwhile, Table 4 shows the variation of r and m, free surface temperature $\theta\left(1\right)$, and heat transfer $-\theta'(0)$ for nanofluid conditions $(\phi_1 = 0.02, \phi_2 = 0)$. The current numerical values of $\theta(1)$ and $-\theta'(0)$ are compared with the results reported by Aziz & Hashim (2010), which shows an excellent agreement. This validation further confirms the accuracy, consistency, and computational stability of the implemented numerical scheme.

Table 3: Comparison value of $-\theta'(0)$ and $\theta(1)$

Pr	$-\theta'(0)$			$\theta(1)$		
	Wang (2006)	Aziz & Hashim (2010)	Present	Wang (2006)	Aziz & Hashim (2010)	Present
1	3.59597	3.591125	3.59599109	0.097884	0.097956	0.09788417
2	5.24415	5.074186	5.25918687	0.024941	0.025083	0.02486247
3	6.51444	5.926547	6.53370208	0.008785	0.008545	0.00831106

Table 4: Comparison value of $-\theta'(0)$ and $\theta(1)$ with Aziz & Hashim (2010)

r	m	$-\theta'(0)$		$\theta(1)$	
		Aziz & Hashim (2010)	Present	Aziz & Hashim (2010)	Present
0	0	0	0	1	1
0	1	1.970409	1.97313728	0.262479	0.26255854
1	0	1.486716	1.48942534	0.548568	0.54879974
1	1	2.677204	2.68096561	0.187817	0.18783952
1	2	3.366711	3.37502673	0.093570	0.09107921
2	0	2.417727	2.42159920	0.347199	0.34734014
2	1	3.277537	3.28206217	0.139192	0.13918317
2	1.5	3.591125	3.59599109	0.097958	0.09788417

Table 5 displays the Carreau hybrid nanofluid's and Carreau nanofluid's variation values for r, m, free surface temperature $\theta(1)$ and heat transfer $-\theta'(0)$ as M rises. We observe that when M increases if r is raised and m remains unchanged (or if r remains unchanged and m is raised), the heat transfer $-\theta'(0)$ rises while the surface temperature decreases for both fluid types. Nanofluids consistently exhibit higher heat transfer rates and lower surface temperatures compared to hybrid nanofluids. From a physical perspective, the variation with M is governed by the interaction between convective transport and magnetic damping. Additionally, the heat transfer is highest when $M = -1$ and decreases as M increases, while the surface temperature shows the opposite trend. It is because of the negative Hartmann number corresponding to the opposing influence of the magnetic field on the fluid flow, which enhances the convection and improves heat transfer. Hybrid nanofluids enhance the heat transfer rate by approximately 4–6% compared to TiO_2–water nanofluids across the investigated magnetic field and rheological parameter ranges. This enhancement can be attributed to the combined effect of improved thermal conductivity and modified rheological behavior associated with the hybrid nanoparticle composition, which influences both energy transport and momentum diffusion. Meanwhile, the increase in heat transfer under negative magnetic field values is attributed to the opposing Lorentz force, which accelerates the fluid motion and enhances convective heat transport. Overall, the results demonstrate that the combined influence of magnetic field strength, surface temperature variation parameters (r,m), and Carreau non-Newtonian effects provides a controllable mechanism for regulating heat transfer performance in electrically conducting thin film flows.This behavior suggests that magnetic field polarity can be strategically used to control thermal performance in electrically conducting thin film systems.

Table 5: Variation of $-\theta'(0)$ and $\theta(1)$ for various values of M , r and m when $\omega = 0.8, \Pr = 6.2, We = 0.2$ and $n = 1$

M	r	m	Hybrid Nanofluid		Nanofluid $(\phi_1 = 0.02, \phi_2 = 0)$	
			$-\theta'(0)$	$\theta(1)$	$-\theta'(0)$	$\theta(1)$
-1	0	1	9.72261800	3.19675×10^{-05}	11.3373627	3.55909×10^{-06}
	1	0	9.96820830	0.000638776	11.69218271	0.000101253
	1	1	13.24138708	5.88309×10^{-06}	15.44739574	4.87905×10^{-07}
	1	2	15.78996268	2.73321×10^{-07}	18.39288676	1.44243×10^{-08}
	2	0	13.53814533	5.8952×10^{-05}	15.83051404	6.60881×10^{-06}
	2	1	16.09033644	1.33145×10^{-06}	18.76746818	8.77807×10^{-08}
	2	1.5	17.20869830	3.1239×10^{-07}	20.05899338	1.63584×10^{-08}
0	0	1	4.98216937	0.011670351	5.21515340	0.008890240
	1	0	4.85324352	0.072079426	5.11523795	0.059046585
	1	1	6.76187214	0.004949227	7.08148321	0.003620887
	1	2	8.14362038	0.000946634	8.51872135	0.000645491
	2	0	6.78973371	0.020092780	7.12754642	0.015526975
	2	1	8.22525667	0.002344010	8.61340447	0.001656591
	2	1.5	8.83529657	0.001056100	9.24742219	0.000721677
1	0	1	3.77193622	0.04486816	3.89784631	0.039153292
	1	0	3.48726960	0.187933578	3.63208971	0.171516800
	1	1	5.10728629	0.023605396	5.27950721	0.020155389
	1	2	6.19724090	0.006534229	6.39896561	0.005367059
	2	0	5.03907021	0.072144931	5.22352037	0.063645651
	2	1	6.21623644	0.013441234	6.42538887	0.011264709
	2	1.5	6.69995022	0.007221581	6.92180305	0.005940672

Figure 2 illustrates the temperature profiles $\theta(\eta)$ for both TiO_2 nanofluid (dashed lines) and Cu– TiO_2 hybrid nanofluid (solid lines) for various magnetic field parameter M values (ranging from -1 to 1). As the distance from the surface η increases, the temperature gradually decreases for both fluids. Near the surface, the hybrid nanofluid maintains approximately 4–6% higher temperature levels compared to the nanofluid, reflecting enhanced thermal conductivity due to the synergistic effect of Cu and TiO_2 nanoparticles. The observed temperature behavior is strongly influenced by the coupled interaction between Carreau non-Newtonian rheology and the applied magnetic field. The Lorentz force generated by a positive magnetic field suppresses fluid motion (damping effect), which weakens convective heat transport and results in a thicker thermal boundary layer with higher temperature retention within the fluid. In contrast, negative values of M enhance fluid motion, strengthening convective heat transfer and promoting a faster decay of temperature away from the surface.

A higher magnetic field, causes a greater reduction in fluid motion through Lorentz forces, leading to lower temperatures, while negative M values increase fluid flow and heat transfer, raising the temperature near the surface. From a rheological perspective, the shear-dependent viscosity of the Carreau fluid further modifies this interaction, where reduced effective viscosity near the surface enhances thermal transport, while increased viscosity away from the surface intensifies the magnetic damping effect on heat transfer. This behavior demonstrates the potential of magnetic field modulation for controlling heat transfer in thin film systems. Overall, the hybrid nanofluid demonstrates superior heat retention compared to the nanofluid, with the magnetic field affecting the heat transfer and flow in expected ways. The combined Carreau–MHD mechanism therefore provides a controllable balance between thermal diffusion and convection, which is essential for optimizing heat transfer performance in non-Newtonian hybrid nanofluid systems.

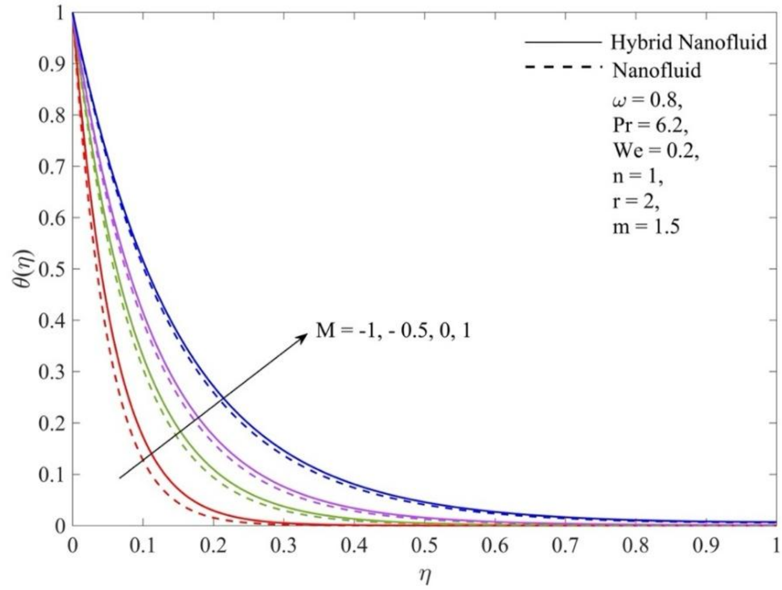

Figure 2: Dimensionless temperature profiles $\theta(\eta)$ for Cu–TiO_2 hybrid nanofluid (solid lines) and TiO_2 nanofluid (dashed lines) for various values of M

Figure 3 illustrates the velocity profiles $f'(\eta)$ of TiO_2 nanofluid (dashed lines) and Cu–TiO_2 hybrid nanofluid (solid lines) under various magnetic field values $(M = -1, -0.5, 0, 1)$. As the distance from the surface η increases, the velocity decreases for both fluids. A positive magnetic field $(M > 0)$ reduces the fluid's velocity because the magnetic force resists its motion, resulting in a velocity reduction of approximately 10–15% near the surface. In contrast, negative magnetic field values enhance flow acceleration. This behavior is further influenced by the Carreau non-Newtonian characteristics of the fluid, where the effective viscosity depends on the local shear rate. In high-shear regions near the stretching surface, the Carreau fluid exhibits reduced effective viscosity, which enhances momentum diffusion and partially offsets the resistive Lorentz force imposed by the magnetic field. Conversely, in low-shear regions away from the surface, the effective viscosity increases, thereby strengthening the damping effect of the magnetic field and leading to a more pronounced velocity decay.

Across all cases, the hybrid nanofluid exhibits 8–12% higher velocities than the TiO_2 nanofluid, indicating superior momentum transport capability, which is beneficial for maintaining stable and uniform thin film flow. This enhancement is attributed not only to improved thermophysical properties but also to the modified rheological response of the hybrid nanofluid, which allows more efficient interaction between shear-dependent viscosity and magnetic forces. The hybrid nanofluid consistently shows higher velocities than the regular nanofluid, due to its improved properties, making it more efficient at maintaining flow. The marked point $(0.494949, 0.316794)$ indicates where the velocities of both fluids briefly match, but beyond that, the hybrid nanofluid again performs better. This demonstrates how the magnetic field affects the flow and why the hybrid nanofluid is superior in promoting faster fluid movement. Overall, the observed trends demonstrate that the coupled Carreau–MHD interaction governs the velocity distribution through a balance between shear-dependent viscosity and electromagnetic damping, providing an effective mechanism for controlling flow behavior in thin film systems.

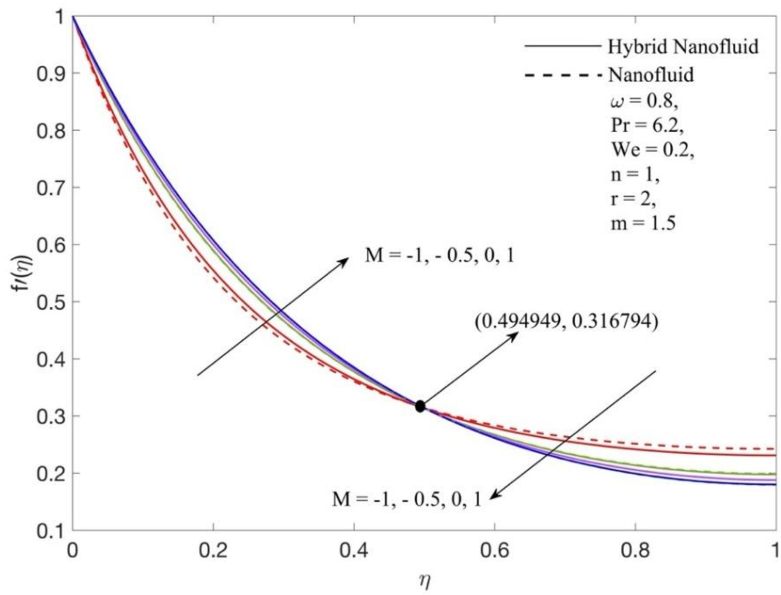

Figure 3: Dimensionless velocity profiles $f'(\eta)$ for Cu–TiO_2 hybrid nanofluid (solid lines) and TiO_2 nanofluid (dashed lines) for various values of M

Compared to a Newtonian fluid, where viscosity remains constant throughout the flow field, the Carreau shear-thinning behavior introduces a spatial variation in effective viscosity that significantly modifies the magnetic damping mechanism. In Newtonian fluids, the Lorentz force produces a relatively uniform suppression of the velocity field due to constant viscous resistance. In contrast, the Carreau fluid exhibits reduced effective viscosity in high-shear regions near the stretching surface, which weakens the relative influence of the Lorentz force and allows higher velocities to persist even in the presence of a magnetic field. This distinction implies that magnetic damping is non-uniform in Carreau fluids is less pronounced near the surface where shear rates are high, but becomes increasingly dominant farther from the surface where the effective viscosity rises. Consequently, the Carreau fluid demonstrates a spatially varying response to magnetic forcing, unlike the more uniform damping behavior observed in Newtonian fluids.

Table 6 shows that as the Hartmann number (M) rises, both the film thickness (R) and skin friction coefficient diminishes for both fluid types. This trend indicates that increasing magnetic field strength suppresses fluid motion through the Lorentz force, leading to a thinner film and reduced momentum development near the surface. At $M = -1$, the film thickness is much larger, but it gets smaller as M rises, with hybrid nanofluids having slightly lower values than nanofluids. Hybrid nanofluids reduce film thickness by approximately 2–3%, which is advantageous for coating uniformity and surface control. The skin friction also becomes less negative as M increases, indicating a reduction in surface shear due to the suppressive Lorentz force. Physically, this reduction in shear stress is associated with weakened velocity gradients at the wall, as magnetic damping limits fluid acceleration within the boundary layer. Comparing hybrid nanofluids with traditional nanofluids, hybrid nanofluids have slightly elevated skin friction, indicating more resistance to fluid flow at the surface. This behavior reflects the modified effective viscosity and enhanced momentum interaction induced by hybrid nanoparticles, which influence the near-wall shear characteristics. Slightly higher skin friction values observed for hybrid nanofluids indicate increased surface shear, which promotes better adhesion in coating and extrusion applications. It should be noted that the magnitude of the Hartmann number represents the strength of the applied magnetic field, while its sign indicates the direction of the magnetic field relative to the flow. A positive Hartmann number corresponds to a magnetic field orientation that induces a Lorentz force opposing the flow motion, whereas a negative Hartmann number represents a reversed magnetic field direction that assists the flow. Consequently, negative values of M enhance fluid motion and increase film thickness, while positive values intensify magnetic damping and reduce both film thickness and wall shear effects. Thus, negative values of the Hartmann number reflect a change in magnetic field orientation rather than a physically negative magnetic field strength.

Table 6: Numerical approximations for the dimensionless film thickness R and local skin friction coefficient $\mathrm{Re}_x^{1/2} C_{fx}$ for hybrid nanofluid and nanofluid as the Hartmann number M varies, using parameters $\omega = 0.8$, $Pr = 6.2$, $We = 0.2$, $n = 1$, $r = 2$ and $m = 1.5$

M	R		$\mathrm{Re}_x^{1/2} C_{fx}$	
	Hybrid nanofluid $(\phi_1 = 0.02, \phi_2 = 0.01)$	Nanofluid $(\phi_1 = 0.02, \phi_2 = 0)$	Hybrid nanofluid $(\phi_1 = 0.02, \phi_2 = 0.01)$	Nanofluid $(\phi_1 = 0.02, \phi_2 = 0)$
–1	15.97934530	20.73079363	–7.25266473	–7.51716659
–0.5	6.75182676	7.33205441	–6.09020460	–5.96686289
0	4.36524873	4.57263356	–5.78617952	–5.63970062
1	2.57533460	2.62928675	–5.56030553	–5.41156700
5	0.98092321	0.97929737	–5.36189067	–5.22061700

Figure 4 represents the temperature profiles $\theta(\eta)$ of TiO_2 nanofluid (dashed lines) and Cu–TiO_2 hybrid nanofluid (solid lines) for various the power-law index n values, which ranges from 0 to 2.5. Fluid behavior is influenced by the power law index n, with $n = 0$ representing a Newtonian fluid and higher values indicating non-Newtonian behavior. As n increases, the temperature decreases more slowly with distance from the surface, meaning the fluid retains more heat. This trend indicates a thickening of the thermal boundary layer as the fluid exhibits stronger non-Newtonian characteristics. The hybrid nanofluid consistently shows higher temperatures, with an enhancement of approximately 5% relative to the nanofluid, indicating its better heat retention due to enhanced thermal conductivity. From a physical perspective, increasing n modifies the shear-dependent viscosity of the Carreau fluid, which reduces the rate of thermal diffusion away from the surface and enhances energy retention within the film. This behavior highlights the combined effect of non-Newtonian rheology and hybrid nanoparticle composition in improving thermal energy storage within the thin film. The zoomed-in section highlights the superior performance of the hybrid nanofluid, even at small scales. This localized enhancement reflects the stronger coupling between momentum and thermal transport induced by hybrid nanoparticles, which sustains higher temperature levels near the surface. Overall, as the fluids become more non-Newtonian with higher n values, the hybrid nanofluid proves more effective at maintaining heat, making it advantageous in applications that require efficient thermal management. These results demonstrate that the power-law index plays a critical role in controlling thermal boundary layer behavior through its influence on viscosity variation and heat transport mechanisms.

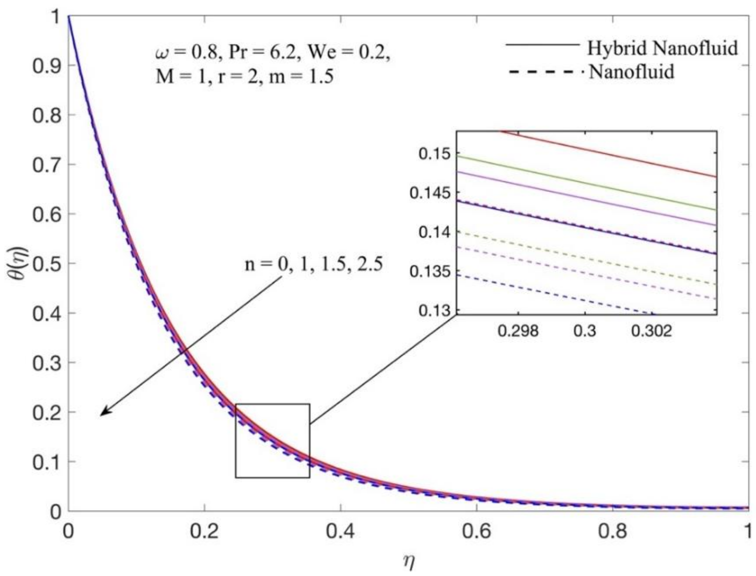

Figure 4: Dimensionless temperature profiles $\theta(\eta)$ for Cu–TiO_2 hybrid nanofluid (solid lines) and TiO_2 nanofluid (dashed lines) for various values of n

Figure 5 shows the velocity profiles $f'(\eta)$ of TiO_2 nanofluid (dashed lines) and Cu–TiO_2 hybrid nanofluid (solid lines) for various power-law index values (n ranging from 0 to 2.5). Fluid behavior is influenced by the power-law index n, with higher n values (such as 2.5) indicating stronger non-Newtonian characteristics. From a rheological perspective, increasing modifies the shear-dependent viscosity of the Carreau fluid, which reduces fluid mobility and leads to a gradual decrease in velocity throughout the boundary layer. The hybrid nanofluid consistently has higher velocities relative to the nanofluid due to its enhanced flow properties. Velocity profiles indicate that hybrid nanofluids maintain 6–10% higher velocities, even as shear-thinning effects become dominant. This enhanced velocity is attributed to the improved momentum transport and modified effective viscosity associated with hybrid nanoparticle interactions, which facilitate more efficient flow despite increased non-Newtonian resistance. The zoomed-in sections highlight that even at small scales, the hybrid nanofluid maintains higher velocities than the nanofluid. The marked point (0.442761, 0.351941) shows where both fluids have the same velocity, but beyond this, the hybrid nanofluid resumes its superior flow. This intersection indicates a transitional region where the competing effects of shear-dependent viscosity and nanoparticle-induced momentum enhancement momentarily balance each other. Thus, the hybrid nanofluid demonstrates better flow behavior, making it more effective for applications requiring smooth fluid movement. Overall, the results demonstrate that the power-law index plays a critical role in controlling velocity distribution through its influence on viscosity variation and momentum diffusion within the thin film.

Table 7 displays how the power-law index n affects the local skin friction coefficient and the dimensionless film thickness (R) for hybrid nanofluids and nanofluids. As n increases from 0 to 2.5, both the skin friction coefficient $\mathrm{Re}_x^{1/2} C_{fx}$ and the film thickness (R) increases for both fluid types, indicating a stronger influence of non-Newtonian rheology on flow resistance and film development. From a physical standpoint, increasing n alters the shear-dependent viscosity of the Carreau fluid, leading to greater resistance to deformation and enhanced momentum diffusion within the film. Quantitatively, the dimensionless film thickness increases by approximately 5–6% over the examined range of n, indicating enhanced resistance to deformation in more non-Newtonian fluids. The film thickness is consistently slightly higher for nanofluids compared to hybrid nanofluids. For instance, at $n = 2.5$, the film thickness of the nanofluid exceeds that of the hybrid nanofluid by approximately 2.0%, highlighting the improved momentum diffusion associated with hybrid nanoparticle inclusion. The local skin friction becomes more negative as n increases, indicating greater resistance to fluid flow, with hybrid nanofluids showing slightly more negative values than nanofluids. This increase in wall shear stress is associated with steeper velocity gradients near the surface, resulting from the modified rheological response of the Carreau fluid at higher n values. Hybrid nanofluids exhibit marginally higher surface shear compared to nanofluids, which can be attributed to the combined rheological effects of Carreau non-Newtonian behavior and enhanced effective viscosity induced by hybrid nanoparticles. Thus, the results demonstrate that the power-law index serves as a key parameter in controlling both film thickness and wall shear characteristics, through its influence on shear-dependent viscosity and momentum transport mechanisms. Overall, higher n values lead to thicker films and greater friction at the surface, suggesting that careful control of the power-law index is essential for optimizing flow resistance and film uniformity in coating and extrusion applications.

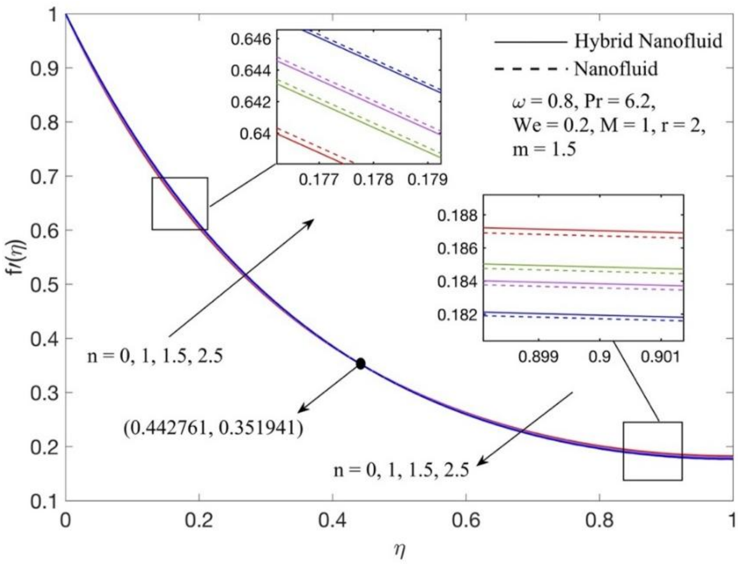

Figure 5: Dimensionless velocity profiles $f'(\eta)$ for various values of n

Table 7: Numerical approximations for the dimensionless film thickness R and local skin friction coefficient $\mathrm{Re}_x^{1/2} C_{fx}$ for hybrid nanofluid and nanofluid as the power-law index n varies, using parameters $\omega = 0.8$, $M = 1$, $Pr = 6.2$, $We = 0.2$, $r = 2$ and $m = 1.5$.

n	R		$\mathrm{Re}_x^{1/2} C_{fx}$	
	Hybrid nanofluid $(\phi_1 = 0.02, \phi_2 = 0.01)$	Nanofluid $(\phi_1 = 0.02, \phi_2 = 0)$	Hybrid nanofluid $(\phi_1 = 0.02, \phi_2 = 0.01)$	Nanofluid $(\phi_1 = 0.02, \phi_2 = 0)$
0	2.51396523	2.56793614	−5.04892185	−4.91282541
1	2.57533469	2.62928675	−5.56030553	−5.41156700
1.5	2.60464210	2.65861400	−5.82207259	−5.66707967
2.5	2.66097554	2.71502718	−6.36106381	−6.19351240

Figure 6 demonstrates the temperature profiles $\theta(\eta)$ of TiO_2 nanofluid (dashed lines) and Cu– TiO_2 hybrid nanofluid (solid lines) at various levels of unsteadiness, represented by ω

(ranging from 0.2 to 1.2). The higher the value of ω, the more unsteady the flow, and as ω increases, the temperature decreases more slowly with distance from the surface, indicating enhanced thermal retention within the thin film. This behavior indicates that stronger unsteadiness intensifies the stretching rate of the surface, which alters the balance between convective and diffusive heat transport within the boundary layer. This behavior arises from the intensified temporal stretching, which suppresses thermal diffusion away from the surface and modifies the structure of the thermal boundary layer. The hybrid nanofluid consistently retains more heat than the nanofluid across all values of ω, as shown by the higher temperature profiles of the solid lines. Quantitatively, the hybrid nanofluid exhibits approximately 4–6% higher temperature levels near the surface compared to the nanofluid, particularly under strongly unsteady conditions. This enhancement is associated not only with improved thermal conductivity but also with the modified rheological response of the Carreau fluid, which influences energy transport under time-dependent stretching conditions. This enhancement is attributed to the superior effective thermal conductivity resulting from the combined presence of Cu and TiO_2 nanoparticles. Thus, both fluids experience a monotonic temperature decay with increasing distance from the surface; however, the hybrid nanofluid demonstrates greater thermal resilience under increasing unsteadiness, suggesting improved performance in transient thermal processes such as thin film coating, rapid cooling, and time-dependent thermal management systems. Overall, the results demonstrate that the unsteadiness parameter plays a critical role in controlling thermal boundary layer development by regulating stretching dynamics, residence time, and heat transport mechanisms within the thin film.

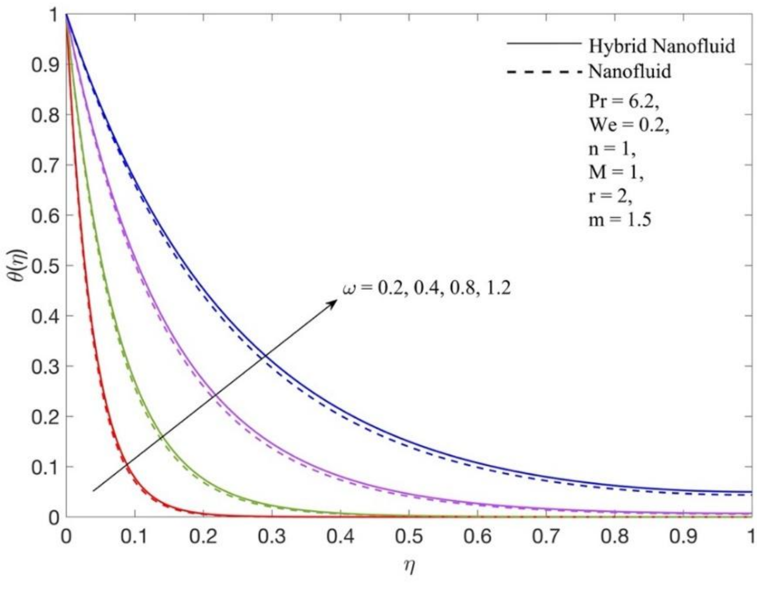

Figure 6: Dimensionless temperature profiles $\theta(\eta)$ for Cu–TiO_2 hybrid nanofluid (solid lines) and TiO_2 nanofluid (dashed lines) for various values of ω

Figure 7 shows the velocity profiles $f'(\eta)$ of TiO_2 nanofluid (dashed lines) and Cu– TiO_2 hybrid nanofluid (solid lines) for various unsteadiness values (ω) ranging from 0.2 to 1.2. Higher ω values represent more unsteady flow conditions. As ω increases, the velocity of both fluids decreases more quickly with distance from the surface, indicating stronger temporal effects that suppress momentum diffusion. This trend reflects the intensification of the stretching rate, which reduces the time available for momentum to diffuse into the fluid and leads to a thinner hydrodynamic boundary layer. This reduction in velocity is associated with enhanced unsteady stretching, which limits the development of the hydrodynamic boundary layer and increases flow resistance. The hybrid nanofluid consistently shows elevated velocities relative to the nanofluid because of its better flow properties and higher thermal conductivity due to the presence of multiple nanoparticles. Quantitatively, the near-wall velocity of the hybrid nanofluid is approximately 8–12% higher than that of the nanofluid, even under strongly unsteady conditions. This enhancement is attributed to the combined influence of improved momentum transport and the shear-dependent viscosity of the Carreau fluid, which allows the hybrid nanofluid to better sustain flow under rapidly varying stretching conditions. This behavior arises from the improved effective viscosity and enhanced momentum transport induced by the synergistic interaction of Cu and TiO_2 nanoparticles. The zoomed-in section highlights that even at small scales, the hybrid nanofluid outperforms the regular nanofluid. From a physical standpoint, the interplay between unsteadiness and non-Newtonian rheology governs the velocity distribution, where time-dependent stretching controls boundary layer development while shear-dependent viscosity modulates momentum diffusion. From an application perspective, this enhanced velocity retention under unsteady conditions is particularly beneficial for processes such as thin film coating, extrusion, and transient cooling systems, where stable flow behavior is essential to ensure uniform film formation and consistent heat removal.

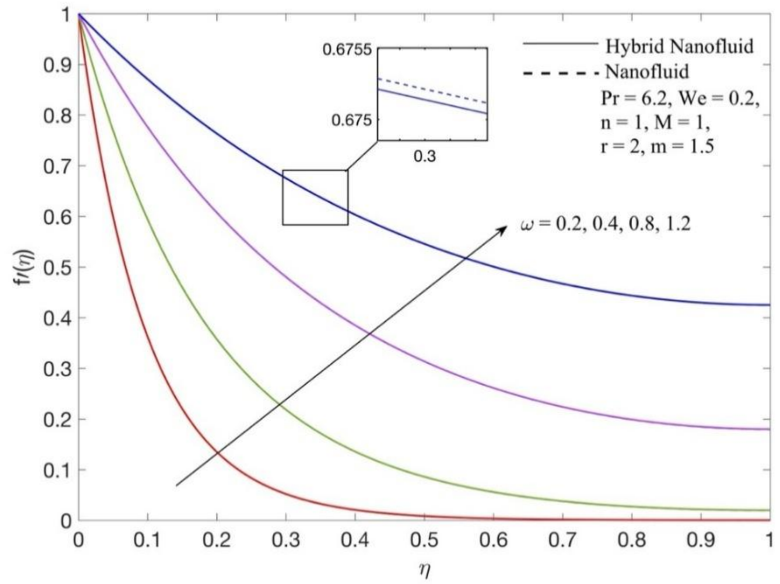

Figure 7: Dimensionless velocity profiles $f'(\eta)$ for Cu–TiO_2 hybrid nanofluid (solid lines) and TiO_2 nanofluid (dashed lines) for various values of ω

Table 8 shows how the unsteadiness parameter ω affects the local skin friction coefficient and dimensionless film thickness (R) for both hybrid nanofluids and nanofluids. As ω decreases from 1.5 to 0.2, the film thickness (R) significantly increases, meaning the fluid layer becomes thicker. This trend indicates that weaker unsteadiness (lower ω) reduces the stretching rate of the surface, allowing the fluid to accumulate and form a thicker film. Quantitatively, the dimensionless film thickness R increases by more than an order of magnitude over this range of ω, demonstrating the strong sensitivity of thin film behavior to flow unsteadiness. At the same time, the skin friction coefficient $\mathrm{Re}_x^{1/2} C_{fx}$ becomes more negative, indicating higher surface friction as the unsteadiness decreases. Physically, this increase in surface shear is associated with enhanced viscous effects due to prolonged fluid residence near the surface, which intensifies momentum exchange within the boundary layer. Across all values of ω, nanofluids have slightly larger film thickness and less negative skin friction than hybrid nanofluids, meaning nanofluids experience less surface friction. For instance, at $\omega = 0.2$, the film thickness R of the nanofluid exceeds that of the hybrid nanofluid by approximately 1–2%, highlighting the improved momentum diffusion and surface control associated with hybrid nanoparticle inclusion. From a rheological perspective, the Carreau non-Newtonian behavior further modulates this response, as the shear-dependent viscosity influences how momentum is distributed under varying unsteady stretching conditions. Thus, lower ω values lead to thicker films and more friction at the surface. Overall, the results demonstrate that the unsteadiness parameter serves as a key control mechanism for tuning film thickness and wall shear, through its combined influence on stretching dynamics, residence time, and viscous transport. From an engineering perspective, these results indicate that unsteadiness serves as an effective control parameter for regulating film thickness R and surface shear, which is critical in coating processes, extrusion technologies, and transient thermal management applications.

Table 8: Numerical approximations for the dimensionless film thickness R and local skin friction coefficient $\mathrm{Re}_x^{1/2} C_{fx}$ for hybrid nanofluid and nanofluid as the unsteadiness parameter ω varies, using parameters $M = 1,\ Pr = 6.2,\ We = 0.2,\ n = 1,\ r = 2$ and $m = 1.5$

ω	R		$\mathrm{Re}_x^{1/2} C_{fx}$	
	Hybrid nanofluid $(\phi_1 = 0.02, \phi_2 = 0.01)$	Nanofluid $(\phi_1 = 0.02, \phi_2 = 0)$	Hybrid nanofluid $(\phi_1 = 0.02, \phi_2 = 0.01)$	Nanofluid $(\phi_1 = 0.02, \phi_2 = 0)$
1.5	0.32240401	0.33163048	−1.76141156	−1.71628421
1.2	0.79850592	0.81901180	−3.06307857	−2.98348369
0.8	2.57533469	2.62928675	−5.56030553	−5.41156700
0.4	12.02254091	12.22666371	−11.4149543	−11.10566003
0.2	48.98809797	49.80422480	−22.2572397	−21.67037942

Furthermore, Figure 8 illustrates the impact of power indice r and m on the temperature distribution $\theta(\eta)$ of the thin film flow. These parameters govern the spatial and temporal variations of the surface temperature, where r controls the spatial stretching rate and m characterizes the temporal evolution of the stretching process. The temperature behavior at the free temperature is highly influenced by both parameters. An increase in either r or m results in a more rapid decay of temperature away from the surface, indicating enhanced thermal boundary layer thinning. From a physical perspective, higher values of r intensify spatial temperature gradients along the surface, while increased m accelerates temporal cooling effects, both of which promote stronger heat transfer from the fluid to the surface. Infer that for both mono and hybrid nanofluids, raising the value of r (or m) will result in a decrease in the free temperature of the thin film flow. Quantitatively, increasing r or m leads to a noticeable reduction in the free surface temperature for both mono and hybrid nanofluids, with the hybrid nanofluid consistently maintaining slightly higher temperature levels due to its superior effective thermal conductivity. This persistent temperature elevation in hybrid nanofluids reflects enhanced energy retention resulting from the synergistic interaction of Cu and TiO_2 nanoparticles. In the absence of m (or r), variations in r (or m) alone are still sufficient to reduce the temperature field, demonstrating that both spatial and temporal stretching mechanisms independently contribute to thermal boundary layer thinning. Overall, the combined influence of r and m provides a flexible mechanism for controlling thermal transport by simultaneously modifying spatial temperature gradients and time-dependent stretching effects. From an engineering perspective, the ability to regulate temperature through the power indices r and m provides an effective mechanism for controlling thermal performance in thin film applications, such as coating, drying, and thermal management systems, where precise temperature regulation is essential.

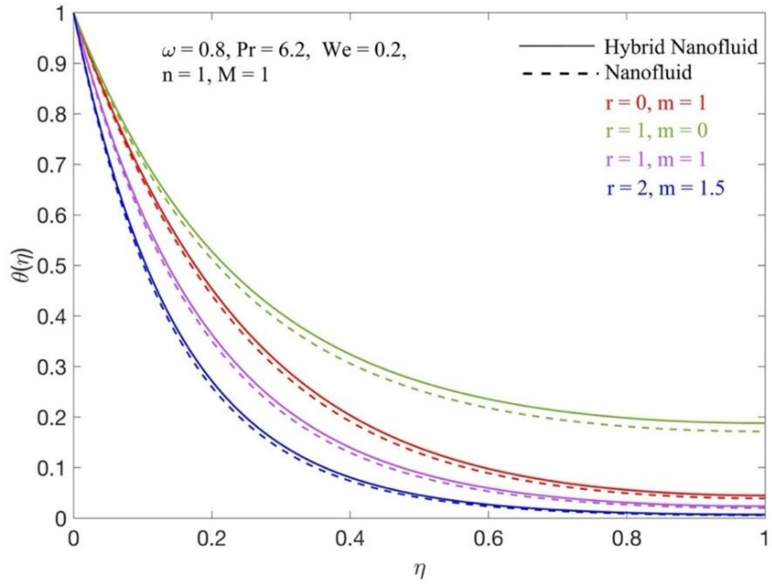

Figure 8: Dimensionless temperature profiles $\theta(\eta)$ for Cu–TiO_2 hybrid nanofluid (solid lines) and TiO_2 nanofluid (dashed lines) for various values of r and m

4. Conclusions

This study comprehensively analyzes MHD Carreau hybrid nanofluid flow over an unsteady stretching surface, using TiO_2 and Cu nanoparticles in a CMC-water base fluid. The results reveal that the hybrid nanofluid enhances velocity by approximately 6–12% and temperature by 4–6% compared to the conventional nanofluid, demonstrating improved momentum and thermal transport performance. In particular, the observed increase in fluid velocity for the hybrid nanofluid should not be attributed to density effects or buoyancy forces, but rather to the combined influence of reduced effective viscosity, enhanced momentum diffusion, and altered Lorentz force interaction arising from hybrid nanoparticle inclusion. Since the present flow is driven by surface stretching and magnetic effects, and buoyancy forces are absent, density alone does not govern the velocity field. The Hartmann number (M) significantly affects the flow, where increasing positive M reduces velocity and heat transfer due to magnetic damping, while negative M enhances flow acceleration and convective heat transfer. Key parameters such as the power-law index (n), and unsteadiness parameter (ω) also play critical roles in controlling flow behavior. Specifically, increasing n and decreasing ω lead to thicker thermal boundary layers and increased surface shear, while higher ω promotes stronger stretching effects that suppress both velocity and temperature profiles. The improved velocity and thermal behavior of the hybrid nanofluid occur despite its higher density, highlighting the dominant role of rheological modification and electromagnetic interaction in controlling the flow. Additionally, hybrid nanofluids reduce film thickness by approximately 2–3% and enhance heat transfer rates by about 4–6%, indicating their effectiveness in improving thin film thermal performance. Hybrid nanofluids demonstrate improved thermal management, reduced film thickness, and higher flow stability due to the combined effects of non-Newtonian rheology and enhanced thermophysical properties.

It is worth noting that the present analysis focuses exclusively on the stretching surface $(b > 0)$.Under these accelerated stretching conditions, the outward momentum transferred from the moving boundary to the fluid prevents flow separation, resulting in a unique boundary-layer solution. Although modern fluid dynamics studies often investigate shrinking surfaces $(b < 0)$, which may produce dual or multiple solutions due to opposing flow dynamics, such conditions are beyond the scope of the present work. From a practical standpoint, continuous coating processes require the substrate to remain under tension for stable operation, making the stretching surface configuration the physically realistic model for this application.

Beyond the specific parametric outcomes, the present results provide broader insights into the design and control of thin film systems involving non-Newtonian hybrid nanofluids. The findings confirm that the coupled effects of Carreau rheology, hybrid nanoparticle interaction, and magnetohydrodynamic forces provide a controllable mechanism for regulating flow and heat transfer behavior. The demonstrated ability to regulate heat transfer, film thickness, and flow stability through magnetic field intensity, unsteadiness, and rheological parameters offers practical guidelines for optimizing coating, extrusion, and thermal management processes. Despite the strong predictive capability of the present model, several simplifying assumptions have been adopted. The effects of nanoparticle agglomeration, sedimentation, temperature-dependent thermophysical properties, and gravitational forces have been neglected to maintain analytical tractability. Consequently, the applicability of the results is primarily limited to thin film flows with moderate temperature variations, low nanoparticle volume fractions, and well-dispersed suspensions. Future research may focus on optimizing nanoparticle volume fractions and hybrid compositions to balance thermal enhancement against flow resistance, as well as extending the present framework to incorporate variable thermophysical properties, surface roughness, gravitational influences, and three-dimensional effects. Experimental validation and transient control strategies based on magnetic field modulation would further strengthen the relevance of the model for real-world industrial deployment. Overall, this study provides a comprehensive and quantitatively supported framework for understanding MHD Carreau hybrid nanofluid thin film flow, offering both theoretical insights and practical guidance for advanced thermal management and surface processing applications.

Acknowledgments

The authors extend their deepest gratitude to Universiti Kebangsaan Malaysia (UKM) for its unwavering support, which was instrumental in facilitating the successful completion of this research. Additionally, the third author would like to express her sincere appreciation to Universiti Malaya (UM) for the continuous support. This research was funded by Tabung Agihan Penyelidikan UKM, grant number TAP-K007136.

Nomenclature

$\mathbf{A}_1$	first Rivlin-Ericksen tensor (Pa)
c	stretching rate (s^{-1})
C_{fx}	local skin friction coefficient $(-)$
C_p	specific heat at constant pressure $(\mathrm{Jkg^{-1}\,K^{-1}})$
CMC	sodium carboxymethyl cellulose $(-)$
Cu	copper $(-)$
d	positive constant (s^{-1})
$f(\eta)$	dimensionless stream function $(-)$
$h(t)$	liquid thin film thickness (m)
$\mathbf{I}$	identity tensor $(-)$
k_f	fluid's thermal conductivity
k_{hnf}	hybrid nanofluid's thermal conductivity
n	power-law index $(-)$
M	the Hartmann number $(-)$
Nu_x	local Nusselt number $(-)$
p	pressure (Pa)
Pr	Prandtl number $(-)$
q_w	wall heat flux $(\mathrm{Js^{-1}\,m^{-2}})$
r	positive power indices $(-)$
m	positive power indices $(-)$
R	unknown constant $(-)$
Re_x	local Reynolds number $(-)$
T	temperature (K)
T_0	temperature at slit (K)
T_w	surface temperature (K)
T_{ref}	reference temperature (K)
TiO_2	Titanium Oxide $(-)$
t	time (s)
u, v	velocity components at $x-$ and $y-$ axes $(\mathrm{ms^{-1}})$
$\mathbf{V}$	velocity fields $(\mathrm{ms^{-1}})$
v_w	uniform surface mass flux $(\mathrm{ms^{-1}})$
We	local Weissenberg number $(-)$
x, y	Cartesian coordinates (m)
Greek symbols	
β	unknown parameter $(-)$
$\dot{\gamma}$	shear rate (s)
ω	unsteadiness parameter $(-)$
η	similarity variable $(-)$
η_∞	high shear rates viscosity $(\mathrm{kg\,m^{-1}s^{-1}})$
η_0	zero shear rates viscosity $(\mathrm{kg\,m^{-1}s^{-1}})$
θ	non-dimensional temperature $(-)$
μ_{hnf}	hybrid nanofluid's dynamic viscosity $(\mathrm{kg\,m^{-1}s^{-1}})$
μ_f	fluid's dynamic viscosity $(\mathrm{kg\,m^{-1}s^{-1}})$
λ	material time constant (s)
ν_f	base fluid's kinematic viscosity $(\mathrm{m^2s^{-1}})$
ρ_{hnf}	hybrid nanofluid's density $(\mathrm{kg\,m^{-3}})$

ρ_f	fluid's density $(\mathrm{kg\,m^{-3}})$
τ	Cauchy stress tensor (Pa)
τ_w	wall shear stress $(\mathrm{kg\,m^{-1}s^{-2}})$
σ_{hnf}	hybrid nanofluid's electrical conductivity $(\mathrm{sm^{-1}})$
σ_f	fluid's electrical conductivity $(\mathrm{sm^{-1}})$
ϕ_1	TiO_2's nanoparticle volume fraction $(-)$
ϕ_2	Cu's nanoparticle volume fraction $(-)$
ϕ_{hnf}	hybrid nanoparticle volume fraction $(-)$
ψ	stream function $(-)$
Subscripts	
w	condition at the stretching sheet's wall
f	base fluid
nf	nanofluid
hnf	hybrid nanofluid
$s1$	TiO_2's solid component
$s2$	Cu's solid component
Superscript	
$'$	derivative with respect to η

References

Abderrahmane A., Qasem N.A.A., Younis O., Marzouki R., Mourad A., Shah N.A. & Chung J.D. 2022. MHD hybrid nanofluid mixed convection heat transfer and entropy generation in a 3-D triangular porous cavity with zigzag wall and rotating cylinder. *Mathematics* **10**(5): 769.

Alabdulhadi S., Abu Bakar S., Ishak A., Waini I. & Ahmed S.E. 2023. Effect of buoyancy force on an unsteady thin film flow of Al2O3/water nanofluid over an inclined stretching sheet. *Mathematics* **11**(3): 739.

Alharbi A.F., Alhawiti M., Usman M., Ullah I., Alam M.M. & Bilal M. 2024. Enhancement of heat transfer in thin-film flow of a hybrid nanofluid over an inclined rotating disk subject to thermal radiation and viscous dissipation. *International Journal of Heat and Fluid Flow* **107**: 109360.

Andersson H.I., Aarseth J.B. & Dandapat B.S. 2000. Heat transfer in a liquid film on an unsteady stretching surface. *International Journal of Heat and Mass Transfer* **43**(1): 69–74.

Aziz R.C. & Hashim I. 2010. Liquid film on unsteady stretching sheet with general surface temperature and viscous dissipation. *Chinese Physics Letters* **27**(11): 110202.

Aziz R.C., Hashim I. & Abbasbandy S. 2018. Flow and heat transfer in a nanofluid thin film over an unsteady stretching sheet. *Sains Malaysiana* **47**(7): 1599–1605.

Bilal M., Saeed A., Gul T., Rehman M. & Khan A. 2021. Thin-film flow of Carreau fluid over a stretching surface including the couple stress and uniform magnetic field. *Partial Differential Equations in Applied Mathematics* **4**: 100162.

Bing Kho Y., Jusoh R., Zuki Salleh M., Hisyam Ariff M. & Zainuddin N. 2023. Magnetohydrodynamics flow of Ag-TiO2 hybrid nanofluid over a permeable wedge with thermal radiation and viscous dissipation. *Journal of Magnetism and Magnetic Materials* **565**: 170284.

Boger D.V. 1977. Demonstration of upper and lower Newtonian fluid behaviour in a pseudoplastic fluid. *Nature* **265**: 126–128.

Carreau P.J. 1972. Rheological equations from molecular network theories. *Transactions of the Society of Rheology* **16**(1): 99–127.

Chabani I., Mebarek-Oudina F., Vaidya H. & Ismail A.I. 2022. Numerical analysis of magnetic hybrid Nano-fluid natural convective flow in an adjusted porous trapezoidal enclosure. *Journal of Magnetism and Magnetic Materials* **564**: 170142.

Chandra Roy N. 2020. Magnetohydrodynamic natural convection flow of a nanofluid due to sinusoidal surface temperature variations. *Physics of Fluids* **32**(2): 022003.

Che Sidik N.A., Adamu I.M. & Mahmud Jamil M. 2020. Preparation methods and thermal performance of hybrid nanofluids. *Journal of Advanced Research in Applied Mechanics* **66**(1): 7–16.

Choi S.U.S. & Eastman J.A. 1995. Enhancing thermal conductivity of fluids with nanoparticles. *Proceedings of the ASME International Mechanical Engineering Congress and Exposition* **231**: 99–105.

Das S. & Jana R.N. 2015. Natural convective magneto-nanofluid flow and radiative heat transfer past a moving vertical plate. *Alexandria Engineering Journal* **54**(1): 55–64.

Gul T., Rehman M., Saeed A., Khan I., Khan A., Nasir S. & Bariq A. 2021. Magnetohydrodynamic impact on Carreau thin film couple stress nanofluid flow over an unsteady stretching sheet. *Mathematical Problems in Engineering* **2021**: 8003805.

Iqbal K., Ahmed J., Khan M., Ahmad L. & Alghamdi M. 2020. Magnetohydrodynamic thin film deposition of Carreau nanofluid over an unsteady stretching surface. *Applied Physics A: Materials Science and Processing* **126**(2): 105.

Islam M.S., Islam S. & Siddiki M.N.A.A. 2023. Numerical simulation with sensitivity analysis of MHD natural convection using Cu-TiO2-H2O hybrid nanofluids. *International Journal of Thermofluids* **20**: 100509.

Jalaluddin D.A., Nazar R., Naganthran K. & Hashim I. 2023. Carreau hybrid nanofilm flow over a stretching sheet with suction/injection effect. *Journal of Quality Measurement and Analysis* **19**(3): 41–53.

Janthe P.G., Tawade J.V., Mahmoud H.A., El-Meligy M. & Khan M.I. 2024. Thin film flows on a linearly moving surface with thermocapillary effects and variable heat generation/absorption. *Journal of Radiation Research and Applied Sciences* **17**(4): 101135.

Jazaa Y., Rehman S., Hashim & Albouchi F. 2024. On the enhancement of heat transport and entropy generation of the thin film flow of partially ionized non-Newtonian hybrid nanofluid. *Journal of the Taiwan Institute of Chemical Engineers* **157**: 105412.

Kamis N.I., Jiann L.Y., Shafie S., Khairuddin T.K.A. & Md Basir M.F. 2022. Magnetohydrodynamics boundary layer flow of hybrid nanofluid in a thin-film over an unsteady stretching permeable sheet. *Journal of Nanofluids* **11**(1): 74–83.

Liu I.C. & Andersson H.I. 2008. Heat transfer in a liquid film on an unsteady stretching sheet. *International Journal of Thermal Sciences* **47**(6): 766–772.

Maity S., Ghatani Y. & Dandapat B.S. 2016. Thermocapillary flow of a thin nanoliquid film over an unsteady stretching sheet. *Journal of Heat Transfer* **138**(4): 042401.

Myers T.G. 2005. Application of non-Newtonian models to thin film flow. *Physical Review E - Statistical, Nonlinear, and Soft Matter Physics* **72**(6): 066302.

Naganthran K., Hashim I. & Nazar R. 2020a. Triple solutions of Carreau thin film flow with thermocapillarity and injection on an unsteady stretching sheet. *Energies* **13**(12): 3177.

Naganthran K., Hashim I. & Nazar R. 2020b. Non-uniqueness solutions for the thin Carreau film flow and heat transfer over an unsteady stretching sheet. *International Communications in Heat and Mass Transfer* **117**: 104776.

Naganthran K., Hashim I., Nazar R., Jalaluddin D.A. & Aruchunan E. 2023. Thermocapillarity in cross hybrid nanofilm flow past an unsteady stretching sheet. *Coatings* **13**(4): 702.

Naganthran K., Nazar R., Siri Z. & Hashim I. 2021. Entropy analysis and melting heat transfer in the Carreau thin hybrid nanofluid film flow. *Mathematics* **9**(23): 3092.

Noor N.F.M., Abdulaziz O. & Hashim I. 2010. MHD flow and heat transfer in a thin liquid film on an unsteady stretching sheet by the homotopy analysis method. *International Journal for Numerical Methods in Fluids* **63**(3): 357–373.

Oztop H.F. & Abu-Nada E. 2008. Numerical study of natural convection in partially heated rectangular enclosures filled with nanofluids. *International Journal of Heat and Fluid Flow* **29**(5): 1326–1336.

Rahman M.M. 2011. Locally similar solutions for hydromagnetic and thermal slip flow boundary layers over a flat plate with variable fluid properties and convective surface boundary condition. *Meccanica* **46**(5): 1127–1143.

Rehman S., Idrees M., Shah R.A. & Khan Z. 2019. Suction/injection effects on an unsteady MHD Casson thin film flow with slip and uniform thickness over a stretching sheet along variable flow properties. *Boundary Value Problems* **2019**(1): 26.

Sadiq M.A. 2021. Heat transfer of a nanoliquid thin film over a stretching sheet with surface temperature and internal heat generation. *Journal of Thermal Analysis and Calorimetry* **143**(3): 2075–2083.

Shahzad H. & Alosaimi M. 2026. Rheological and thermal behavior of calendering process of hybrid nanofluid: A magnetohydrodynamic thin film analysis. *Macromolecular Theory and Simulations* **35**(1): e00088.

Shampine L.F., Gladwell I. & Thompson S. 2003. *Solving ODEs with MATLAB*. New York: Cambridge University Press.

Sheik S.B., Nagireddy P.D. & Kupireddi K.K. 2026. A review on synthesis and characterization of hybrid nanofluids for heat exchangers. *Proceedings of the International Conference on Communication and Intelligent Systems*, pp. 457–469.

Sulochana C. & Ashwinkumar G.P. 2017. Carreau model for liquid thin film flow of dissipative magnetic-nanofluids over a stretching sheet. *International Journal of Hybrid Information Technology* **10**(1): 239–254.

Sundar L.S., Singh M.K. & Sousa A.C.M. 2014. Enhanced heat transfer and friction factor of MWCNT-Fe3O4/water hybrid nanofluids. *International Communications in Heat and Mass Transfer* **52**: 73–83.

Suresh S., Venkitaraj K.P., Selvakumar P. & Chandrasekar M. 2011. Synthesis of Al2O3-Cu/water hybrid nanofluids using two step method and its thermo physical properties. *Colloids and Surfaces A: Physicochemical and Engineering Aspects* **388**(1–3): 41–48.
Takabi B. & Salehi S. 2014. Augmentation of the heat transfer performance of a sinusoidal corrugated enclosure by employing hybrid nanofluid. *Advances in Mechanical Engineering* **6**: 147059.
Tayebi T., Öztop H.F. & Chamkha A.J. 2021. MHD natural convection of a CNT-based nanofluid-filled annular circular enclosure with inner heat-generating solid cylinder. *The European Physical Journal Plus* **136**(2): 150.
Thirumalaisamy K. & Reddy A.S. 2023. Numerical computation on MHD natural convective ternary nanofluid flow and heat transfer in a porous square cavity: Marker-and-cell technique. *International Journal of Numerical Methods for Heat & Fluid Flow* **33**(10): 3425–3466.
Ullah A., Alzahrani E., Shah Z., Ayaz M. & Islam S. 2018. Nanofluids thin film flow of Reiner-Philippoff fluid over an unstable stretching surface with Brownian motion and thermophoresis effects. *Coatings* **9**(1): 21.
Ullah A., Guo X., Gul T., Ali I., Saeed A. & Galal A.M. 2023. Thin film flow of the ternary hybrid nanofluid over a rotating disk under the influence of magnetic field due to nonlinear convection. *Journal of Magnetism and Magnetic Materials* **573**: 170673.
Vemula R., Chamkha A.J. & Mallesh M.P. 2016. Nanofluid flow past an impulsively started vertical plate with variable surface temperature. *International Journal of Numerical Methods for Heat and Fluid Flow* **26**(1): 328–347.
Waini I., Ishak A. & Pop I. 2021. MHD Glauert flow of a hybrid nanofluid with heat transfer. *Journal of Advanced Research in Fluid Mechanics and Thermal Sciences* **86**(2): 91–100.
Wang C. 2006. Analytic solutions for a liquid film on an unsteady stretching surface. *Heat and Mass Transfer* **42**(8): 759–766.
Wang C.Y. 1990. Liquid film on an unsteady stretching surface. *Quarterly of Applied Mathematics* **48**(4): 601–610.
Zainal N.A., Nazar R., Naganthran K. & Pop I. 2020a. MHD mixed convection stagnation point flow of a hybrid nanofluid past a vertical flat plate with convective boundary condition. *Chinese Journal of Physics* **66**: 630–644.
Zainal N.A., Nazar R., Naganthran K. & Pop I. 2020b. Unsteady three-dimensional MHD non-axisymmetric homann stagnation point flow of a hybrid nanofluid with stability analysis. *Mathematics* **8**(5): 784.
Zainal N.A., Nazar R., Naganthran K. & Pop, I. 2021. Stability analysis of unsteady MHD rear stagnation point flow of hybrid nanofluid. *Mathematics* **9**(19): 2428.
Zainal N.A., Nazar R., Zuberi H.A. & Pop I. 2025. Enhanced heat transfer in hybrid nanofluid: Role of suction and wedge angle on boundary layer dynamics. *Journal of Quality Measurement and Analysis* **21**(2): 163–174.

Department of Mathematical Sciences
Faculty of Science and Technology
Universiti Kebangsaan Malaysia
43600 UKM Bangi
Selangor, MALAYSIA
E-mail: p109938@siswa.ukm.edu.my, rmn@ukm.edu.my, ishak_h@ukm.edu.my*

Institute of Mathematical Sciences
Faculty of Science
Universiti Malaya
50603 Kuala Lumpur, MALAYSIA
E-mail: kohi@um.edu.my

Received: 30 June 2025
Accepted: 25 April 2026

*Corresponding author